Available online at www.garmian.edu.krd

Passer Journal

Passer 6 (Issue 1) (2024) 92-106

http://passer.garmian.edu.krd/

Lateral Earth Pressure Reduction on High-Filled Cut-and-Cover Tunnels Using Expanded Polystyrene Geofoam and Tire-Derived Aggregate

Shamil Ahmed Flamarz Arkawazi[1], Mohammad Hajiazizi[1*]

[1]*Department of Civil Engineering, Faculty of Engineering, Razi University, Kermanshah, Iran.*

Received 04 March 2023; revised 27 January 2023;
accepted 31 January 2024; available online 31 January 2024

DOI: 10.24271/PSR.2024.433607.1461

ABSTRACT

Currently, high-filled cut-and-cover tunnels (HFCCTs) are a practical solution for the prospect of reclaiming valuable usable lands with valleys and hilly terrain around the world. As a result of the very high backfill soil amount above the HFCCT producing very huge earth pressure, it is essential to use methods of load reduction methods to reduce the earth loads and pressures on the HFCCT, which will increase the safety by reducing the tunnel designing loads. This study focuses on six load reduction scenarios using expanded polystyrene (EPS) and tire-derived aggregate (TDA) in three different forms. The research includes using EPS geofoam and TDA in arch and combined horizontal and arch formations as methods of LEP reduction on HFCCTs which is the first time these methods have been used as methods of any type of load reduction on HFCCTs. A number of significant factors, including the suggested EPS and TDA forms, the EPS and TDA thickness, and the distance between the bottom of the EPS or the TDA and the top of the HFCCT were studied. The study results determined that a significant LEP reduction on the HFCCTs was achieved, especially with the use of TDA in a horizontal form. Also, model verification was made by comparison between the calculated and estimated LEP values on the HFCCT study model using the Rankine equation, Rankine modified equation, and Abaqus CAE 2019 software. The calculated and estimated LEP values showed that the calculated value using the Rankine modified equation is 23.61% lower than the calculated value using the Rankine equation, which is a high percentage of difference. The estimated value using Abaqus CAE 2019 is 47.56% higher than the calculated value using the Rankine equation, which is also a high percentage of difference.

Keywords: High-Filled Cut-and-Cover Tunnels, Lateral Earth Pressure, Expanded Polystyrene, Tire-Derived Aggregate.

1. Introduction

The HFCCTs provide a reasonable and practical solution for the possibility of reclaiming valuable lands with valleys and hilly or mountainous terrain around the world. The basic property of the HFCCTs is their very high or huge backfill soil. However, the ultrahigh high earth pressure induced on the top or side of the HFCCT can cause serious structural damage and problems and safety-related concerns. Studies focusing on the pressure reduction effect in the backfill soil above pipes and culverts have taken place since the early years of the 20th century; but, a few or very limited studies were focusing on HFCCTs-related load and load reduction issues.

Marston initiated the idea and concept of rigid pipes installation in a trench buried under backfill soil. Earth pressure on buried rigid pipes is usually estimated using Marston's theory[1, 2].

* Corresponding author
E-mail address: mhazizi@razi.ac.ir (Instructor).
Peer-reviewed under the responsibility of the University of Garmian.

In 1922 Marston confirmed that the major factor that affects the earth pressure on underground rigid pipes depends on the relative settlement between the soil column (interior prism) above the rigid pipe and the adjacent soil columns (exterior prisms) that control the magnitude and direction of friction, which affecting the earth pressure on the rigid pipe. A compressible material, like baled straw, leaves, woodchips, sawdust, and expanded polystyrene (EPS) geofoam, can be placed above rigid pipes to reduce the earth pressure on the rigid pipes and produce positive soil arching[3-11].

In northwestern China, the HFCCTs are prevalent because the construction of HFCCTs allows the reclaiming of valuable lands. Because of the unique plateau topography of this region of China, the required quantities of backfill soil for HFCCTs are massive, and the backfill must be high enough to increase the usable land area. At present, the main challenge of HFCCTs construction is high earth or ground pressure on the HFCCTs lining structure and related safety concerns[12].

A study was conducted to discuss laboratory experimental tests that were made to examine ways of earth pressure reduction methods by inserting expanded polystyrene (EPS) geofoam into the backfill soil and modifications to the structure of HFCCTs. The results of the experimental tests are in good agreement with the results of the numerical analysis. Numerical analysis was used to determine the optimal thicknesses of EPS to reduce the earth pressure on HFCCT with different backfill heights. Modifying the sectional shape of HFCCT can change the internal forces and make the concrete structure of HFCCT support more compressive loads instead of failing due to bending moments. The results of the study show that the dual effects of load reduction with EPS and sectional modifications of HFCCT can reduce the required thickness of the HFCCT structure, increase the allowable backfill height, and improve HFCCT safety[12].

A research was conducted to describe three load reduction scenarios: using EPS geofoam on the top of the HFCCT; a combination of EPS geofoam on top of the HFCCT and geogrid above the EPS geofoam; and a combination of EPS geofoam on the top of the HFCCT, geogrid above the EPS geofoam, and concrete wedges under the side edges of the geogrid. PFC2D computer software is used to analyze the suggested load reduction scenarios. Significant factors including density, thickness, width, and the location of the EPS geofoam over the HFCCT, in addition to the number of layers and the tensile strength of the geogrid were studied. The analysis results were based on the changes in the VEP, the backfill soil relative vertical displacement, the contact force among the particles of backfill soil, and the geogrid relative vertical displacement. The research results determined that the factors have significant effects on the load reduction mechanisms. To optimize the earth pressure reduction on the top of HFCCTs, the influential factors' optimum values were derived[13].

Better methods to reduce loads on the HFCCTs, which will reduce lining structure and design costs and increase safety, need a good understanding of the load or earth pressure reduction mechanisms. The earth pressure on top of HFCCTs can be reduced using relatively low compacted (RLC) soil, but using the RLC soil layer on the top of HFCCTs makes the load transfer mechanism more complex. The prior studies have either focused on the micromechanical properties of backfill soils or ignored their special properties. Therefore, if the micromechanical properties of the backfill soil can be correctly considered, then the load transfer mechanisms can be better understood. It should be considered to backfill the HFCCTs with soils with different relative compaction (R) percentages, such as R=90% for HFCCT main Backfill soil and R=80% for the RLC layer above the HFCCT[10].

The discrete element method (DEM) was employed to examine and inspect the changes in vertical earth pressure (VEP) on HFCCTs proportional to the thickness and spread distance of the RLC soil layer, the valley width to the width of the HFCCT ratio (the B/D ratio), and the slope angle. To characterize these factors, parametric DEM studies were conducted. The results of the DEM study showed that an adequate thickness and spread distance of the RLC soil layer could optimize the effect of soil arching and reduce VEP on top of HFCCTs. Also, the results showed that the slope angle and B/D ratio are related to the redirect of the VEP[10].

Tire-derived aggregate (TDA) was successfully applied to reduce the earth pressure of backfill soil on a railway CCT. Numerical analyses were conducted to check and examine the effect of different assumptions about the base model with the suggested TDA applying formations around the CCT. Numerical analysis results stated that up to 60% reductions in the tunnel lining structure flexural moment can be achieved. For the studied case, the TDA elastic property has a small effect on CCT lining pressures in spite of it being fundamental for the CCT backfill settlement estimates[14].

A numerical study was conducted to examine two load reduction methods using a combination of TDA and geogrid. Abaqus 2019 software was employed to analyze the LEP reduction progress and mechanism. Several factors, including the geogrid existence, the form of the TDA, the thickness of the TDA, and the distance between the bottom of the TDA and the top of the HFCCT were studied. It was determined that the factors are having significant effects on the LEP reduction on the HFCCT through the earth pressure reduction mechanisms, where the average LEP on the top of the HFCCT model reduced from 303 kPa to 125 kPa[15].

The aim of this study is to investigate the effect of using EPS as compressible crushable material and TDA as compressible material through three scenarios on LEP reduction on HFCCTs. The three scenarios include using EPS and TDA in three different formations:

1- In a horizontal form.

2- In an arch form.

3- In a combined horizontal and arch form.

In the three scenarios, the EPS and TDA are located above the HFCCT concrete lining structure with six thicknesses and three distances between the top of the HFCCT and the bottom of the EPS and TDA. The novelty of this research is using EPS geofoam and TDA in arch and combined horizontal and arch formations as methods of LEP reduction on HFCCTs which is the first time these methods have been used as methods of any type of load reduction on HFCCTs. As the objectives of this study, factors, such as the EPS and TDA formation, the EPS and TDA thickness, and the distance between the top of the HFCCT and the bottom of the EPS and TDA, will be checked and examined. The study results will focus on changes in LEP and relative vertical displacement in the backfill soil prisms.

2. The HFCCT Study Model and Suggested Load Reduction Methods

For purposes of this study, a prototype HFCCT model was selected. The HFCCT study model consists of a 50 m depth valley and two sides slope with 70^{o} angles, a 4-lane road CCT (the CCT height is 7.7 m) is located at the base of a valley. The selected study model can be considered quite challenging in terms of the very high earth pressure applied on the HFCCT produced from the huge backfill soil amount. The HFCCT study model parameters were selected to reflect the natural difficult conditions of valleys and the hilly terrain.

In general, HFCCT has a 30-50 m backfill soil height, such a high soil column produces very high earth pressure on the lining structure of the CCT, and the structure is susceptible to crack, causing damage to the tunnel structure and difficulty in its regular function[16].

Figure 1 shows the cross-section of the HFCCT study model with all the required details and dimensions to conduct the current study.

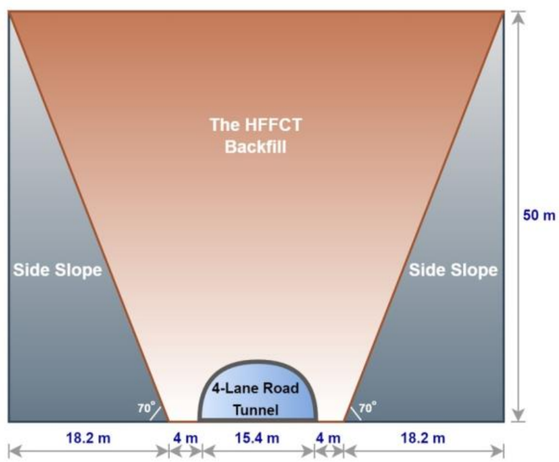

Figure 1: The high-filled cut-and-cover tunnel (HFCCT) study model.

3. Study Materials Parameters

3.1 Backfill Soil Parameters

The required physical and mechanical properties of the backfill soil to conduct this study were determined by conducting the relevant laboratory tests. The internal friction angle, φ, the cohesion, c, and Young's modulus values were determined by performing triaxial compression tests. The backfill soil tests results are shown in Table 1.

Table 1: Engineering properties of backfill soil.

Cohesion (c) (KPa)	Internal friction angle (φ) (°)	Young's modulus (E) (MPa)	Poisson's ratio (ν)	Saturated density (ρ) (Kg/m^3)
7.2	36	11.250	0.3	1870

3.2 Expanded Polystyrene (EPS) Geofoam Parameters

EPS geofoam is a rigid cellular plastic foam that generally has been widely used in civil engineering applications specifically used in geotechnical projects and applications, including stabilization of slopes[17], rapid construction of embankments over compressible soils[18], lateral loads reduction (static and dynamic) on retaining walls and bridge abutments[19-24], as a dynamic loads damper or barrier[25] and as a sub-base filling material[26-29]. Numerical solutions were used to study EPS geofoam composite soil with its physical and engineering properties[30, 31]. The EPS is widely used in geotechnical applications because of its unique properties, such as being lightweight (low density), having different mechanical behavior, and being low in permeability. Several studies have shown that the compressive strength of EPS Geofoam is mainly dependent on material density, confining stress, and strain rate[32-36].

For the past forty years, EPS has been successfully used as construction material in civil engineering projects, especially in the field of geotechnical engineering, due to its wide variety and range of applications, such as in embankments as lightweight filling material and in retaining walls as a compressible inclusion[37].

For research purposes, four different densities of EPS geofoam are selected and purchased from EPS geofoam local suppliers in Mumbai, India. Figure 2(a) shows the EPS geofoam line sketch, and Figure 2(b) shows the photograph of the triaxial test EPS geofoam specimen used in the experimental study tests. The mechanical properties of the EPS geofoam are given and illustrated in Table 2[37].

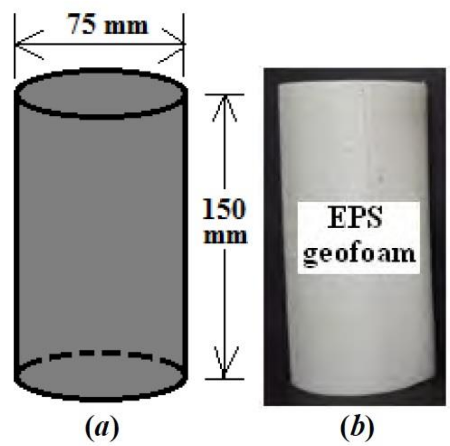

Figure 2: EPS geofoam triaxial test specimen (a) EPS test specimen line sketch and (b) EPS test specimen photograph[37].

Table 2: EPS geofoam mechanical properties[37].

Density (Kg/m^3)	Unit weight (kN/m^3)	Compressive Strength (kPa)	Initial Modulus (kPa)	Tensile Strength (kPa)	Shear Strength (kPa)
15	0.15	61.95	2480.76	154.59	83.65
20	0.20	91.39	4070.55	216.40	94.37
22	0.22	110.53	5508.16	244.54	121.57
30	0.30	146.80	7550.28	407.78	139.27

A standard triaxial loading frame with a triaxial cell to fit a sample with 75 mm diameter and 150 mm height is used to conduct the experimental tests (see Figure 3). The Unconsolidated Un-drained triaxial experimental tests were conducted with a constant strain rate of 1.2 mm/min and were performed according to IS 2720 (Part 11):1993. A load cell and Linear Variable Differential Transducer were used to measure the deviator load and vertical displacement. All the tests were conducted with up to a maximum axial strain of 15%[37].

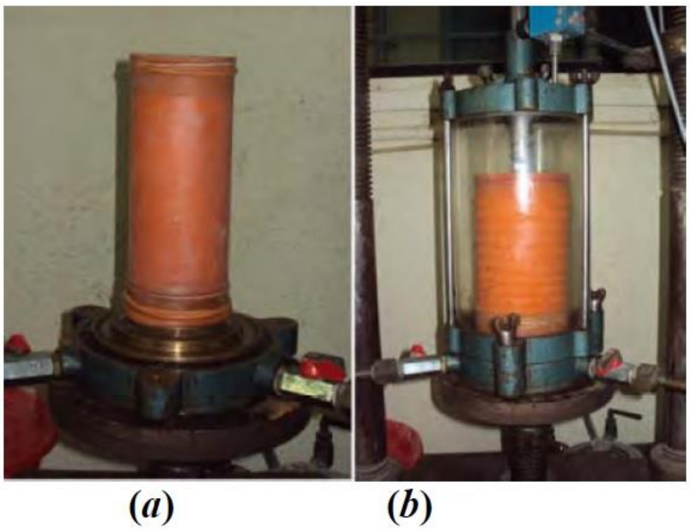

Figure 3: EPS geofoam triaxial test (a) Placement of the testing specimen (b) The specimen during conducting the test[37].

In the testing of the EPS geofoam specimens under triaxial loading conditions, no particular surface failure was observed. It was noticed that the specimens were getting marginal and compressed or small sideways bulging with the increase in the deviator load. In all the EPS geofoam confining pressures and densities, a similar pattern was observed. The EPS geofoam test specimen deformation with different densities is shown in Figure 4[37].

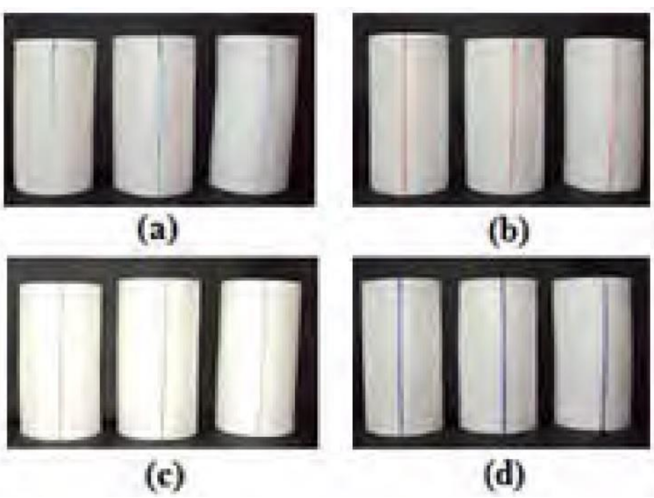

Figure 4: The EPS geofoam test specimen deformation under different confining pressures for different unit weights (a) 0.15 kN/m^3, (b) 0.20 kN/m^3, (c) 0.22 kN/m^3 and (d) 0.30 kN/m^3 [37].

Deviator load was noted or recognized for each increase of axial deformation of EPS geofoam specimen. Deviator stress-strain relationships of the EPS geofoam with different unit weights under different confining pressures are shown in Figure 5. For all the tested unit weights of EPS geofoam, the stress-strain relationship was linear up to the axial strain value of around 2%; later, it was observed that there was no significant change in the deviator stress value with respect to the increase in axial strain value. As the unit weight of the EPS geofoam is increased, the deviator load is increased for all the confining pressures. For all the unit weights and confining pressures, the principal stress difference was almost equal [37].

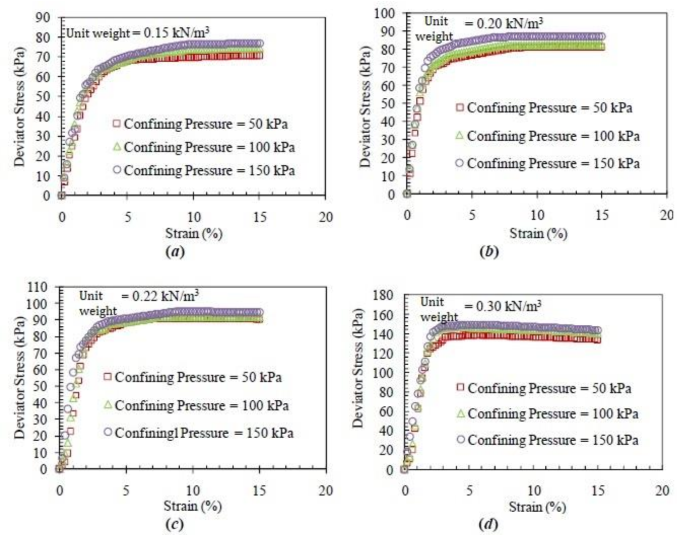

Figure 5: Stress-strain relationship of EPS geofoam under triaxial loading for different unit weights (a) 0.15 kN/m^3, (b) 0.20 kN/m^3, (c) 0.22 kN/m^3, and (d) 0.30 kN/m^3[37].

By constructing Mohr's circles, the EPS geofoam strength parameters of different unit weights were calculated (see Figure 6). The EPS geofoam cohesion value increased with the increase in the unit weight, and there was a slight increase in the internal friction angle. The EPS geofoam strength parameters obtained from the triaxial tests are shown in Table 3. From the strength parameters, it was noticeable that the cohesion value has a considerable effect on the EPS geofoam strength. Figure 7 shows the relation of cohesion values with respect to the EPS geofoam corresponding unit weight. A regression analysis is conducted for different EPS geofoam unit weights and the best fitted to a curve expressed as Equation 1[37].

$$C = 894.7\,\gamma_g^2 - 214.3\,\gamma_g + 45.78 \qquad (1)$$

Where:

C: is the cohesion (kPa).

γ_g: is the unit weight of EPS geofoam (kN/m^3).

Table 3: EPS geofoam shear strength parameters of different unit weights[37].

EPS geofoam unit weights γ_g (kN/m3)	Cohesion C (kPa)	Internal friction angle φ (°)
0.15	33.75	1.5
0.20	38.75	2
0.22	41.88	2
0.30	62.00	2.5

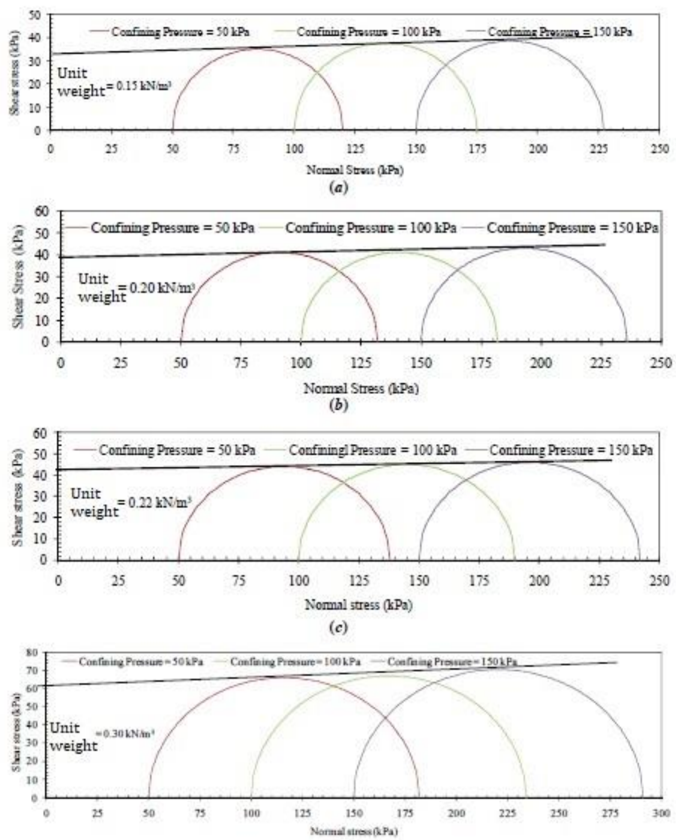

Figure 6: Construction of Mohr's circle for different EPS geofoam unit weights (a) 0.15 kN/m^3, (b) 0.20 kN/m^3, (c) 0.22 kN/m^3 and (d) 0.30 kN/m^3[37].

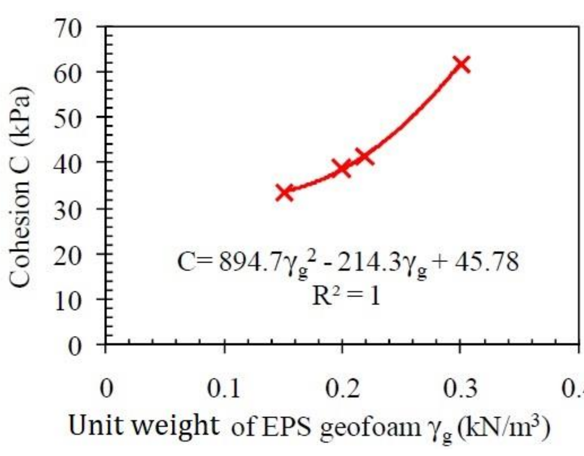

Figure 7: The relation between cohesion and EPS geofoam unit weight[37].

The EPS geofoam Poisson's ratio (υ) value is calculated using Equation 2. The Poisson's ratio (υ) value and other EPS geofoam properties are illustrated in Table 4[37].

$$\upsilon = 0.0056\,\rho + 0.0024 \qquad (2)$$

Where:

ρ: EPS geofoam density (kg/m^3).

Table 4: EPS geofoam mechanical and physical properties[37].

Unit weight γg (kN/m3)	Cohesion C (kPa)	Internal friction angle φ (°)	Young's modulus E (kPa)	Poisson's ratio υ
0.15	33.75	1.5	2400	0.10
0.20	38.75	2	4000	0.12
0.22	41.88	2	5500	0.125
0.30	62.00	2.5	7800	0.17

For the purposes of this study and to achieve the highest relative settlement between the HFCCT backfill soil interior and exterior prisms, the EPS geofoam with a 15 Kg/m^3 density is selected. The mechanical and physical properties of the selected EPS geofoam are given in Table 4.

3.3 Tire-Derived Aggregate (TDA) Parameters

The American Society for Testing and Materials (ASTM) in ASTM D6270-08, "Standard Practice for Use of Scrap Tires in Civil Engineering Applications", provided an inclusive list of terms and definitions and summarized the standard practice for scrap tires used in the applications of civil engineering [38].

Because of the lightweight of the TDA, it has been used as a successful alternative filling material for the embankment. TDA is approximately one-third of the traditional filling materials' weight and thus produces less pressure on the underlying structures or materials. This property is an advantage and can be beneficial when designing embankment filling projects in which the underlying foundation or base soil cannot support the high weight of traditional backfill soil. In addition to the lightweight property of the TDA, it has high permeability and, thus, generally does not demand the placement or use of sub-drain systems, which will provide additional cost savings. In addition to TDA being a successful lightweight filling material, it is also has proven to be a cost-effective alternative to other lightweight materials such as pumice and EPS geofoam. There are other benefits and applications of TDA except using it as filling materials for embankment and road fill, such as increasing the stability of steep slopes along roadways, reinforcing roadway shoulders, and providing an insulating layer against frost penetration due to its properties of thermal resistance. According to the ASTM standard, the TDA is divided into two main types, which are used in engineering applications, Type A and Type B, and two filling classes related to them, Classes I and II. Type A and Type B are two TDA size classifications that are used in various engineering applications. Classes I and II describe the fill of the raised thicknesses as introduced by ASTM D6270-08, Section 6.10.1. Type A TDA material is about 75 to 100 mm in size, and Type B TDA material is 152.4 to 304.8 mm. TDA layers that are less than 1 meter in height are classified as Class I fills, and TDA layers that are between 1 and 3 meters high are classified as Class II fills. Typically, Class I fills use TDA material Type A, and applications requiring TDA material Class II fill use Type B. Table 5 illustrates Type A and Type B size classifications, and Figure 8 shows typical or standard samples of TDA material. TDA is a compressible material. Therefore, the density of TDA varies depending on whether it is installed in the project or stockpiled. The stockpile and shipping densities of TDA material Type A and Type B range from 400.461 to 560.646 kg/m^3, while the compacted in-place density values of TDA material Type A and Type B range from 560.646 to 800.923 kg/m^3 (see Table 6)[39].

Elastic modulus (E) is the proportional coefficient between the applied stress and the measured strain; for example, in the one-dimensional tensile test, the lower E values are indicative of layer deformation. The TDA modulus of elasticity (E) ranges from 1.241 MPa to 5.171 MPa[38]. For comparison, the modulus of elasticity (E) of dense, drained sands can range from 41.368 MPa to 82.737 MPa[40]. The elastic modulus (E) for gravel is a lot larger. Therefore, under the same loading conditions, the TDA will deform much more than the soil. Poisson's ratio (ν) is the ratio of transverse strain to longitudinal strain, as measured, in a one-dimension tensile test, the TDA Poisson's ratio is 0.5[38], which means that the TDA deforms at a constant volume. As a comparison, the Poisson's ratio (ν) for mineral aggregate ranges from 0.15 to 0.45[40].

For the numerical analysis of this study, the required TDA material physical and mechanical properties were selected and summarized in Table 7.

Table 5: TDA fill classes (ASTM D6270-08 Section 6.10.1-4)[39].

Characteristics	TDA Type A	TDA Type B
Fill Class	Class I	Class II
Typical Size	75-100 mm	150-300 mm
Maximum Layer Depth	Less than 1 m	Less than 3 m

Table 6: Densities of type A and type B TDA[39].

Stages	TDA Type A, Kg/m^3	TDA Type B, Kg/m^3
Shipping and Stockpiling	400.461-560.646	400.461-560.646
Compacted	720.830-848.978	720.830-800.923

Figure 8: Left - Type A TDA, Right - Type B TDA[39].

Table 7: TDA physical and mechanical properties[14, 39].

Material	Density (ρ) (Kg/m^3)	Unit weight (γ) (kN/m3)	Young' s modulus (E) (MPa)	Poisson's ratio (ν)	Cohesion C (kPa)	Angle of internal
Backfill soil	1870	18.70	11.25	0.3	7.2	36
EPS geofoam	15	0.15	2.40	0.10	33.75	1.5
TDA	400.461	4.00461	0.63	0.2	10	23

4. Numerical Analysis and Model Creation

The numerical analyses of this study were conducted using Abaqus CAE 2019 software, which is based on the finite element method. For the numerical analyses, a 1/50 scale finite element model of the actual HFCCT study model was created (see Figure 9). In the study finite element model, the valley sides' slopes are assumed to be rigid. To model the HFCCT, the Abaqus CAE Standard/Explicit Model, which uses plane strain element type, is selected. The boundaries at two sides of the study HFCCT finite element model are restrained in horizontal directions using rollers that only vertical displacement is permissible, and the model's bottom boundary is entirely fixed. To model the backfill soil, the Mohr-Coulomb elastoplastic criterion was used. For the EPS geofoam, density, elasticity, cohesion, and angle of internal friction, in addition to the crushable foam model must be defined in Abaqus CAE 2019 to fit the EPS geofoam stress-strain relationship. For the TDA material, the Mohr-Coulomb elastoplastic criterion was used for modeling the properties of the material. In order to achieve accurate numerical analysis results, mesh size and orientation sensitivity tests were investigated. The mechanical and physical parameters used in the finite element analysis, such as the mechanical and physical properties for backfill soil, EPS geofoam, and TDA, are summarized in Table 8.

Table 8: Mechanical and physical properties of the materials required for the finite element analysis.

Density ρ (kg/m3)	Cohesion C (kPa)	Angle of internal friction φ (°)	Modulus of elasticity E (kPa)	Poisson's ratio υ
400.461	10	23	630	0.2

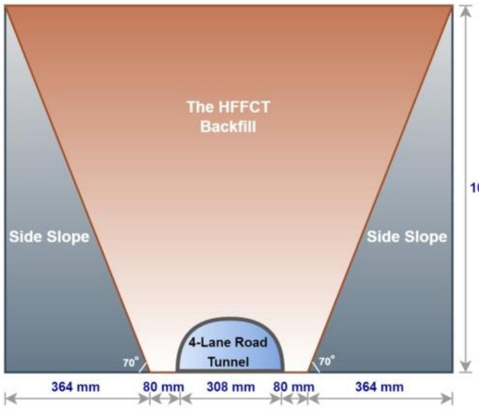

Figure 9: A 1/50 scale created finite element HFCCT model of the actual HFCCT study model.

5. Results of Numerical Analysis

5.1. Lateral Earth Pressure (LEP) Estimation on the HFCCT for the Base Condition of the Study Model (No Load Reduction Method is Used)

A numerical analysis was conducted to determine the average LEP on the finite element HFCCT study model with the base conditions (see Figure 10). The average LEP on the top of the actual HFCCT study model with the base conditions was determined based on the average LEP estimation on the finite element HFCCT model, and its value is 303 kPa.

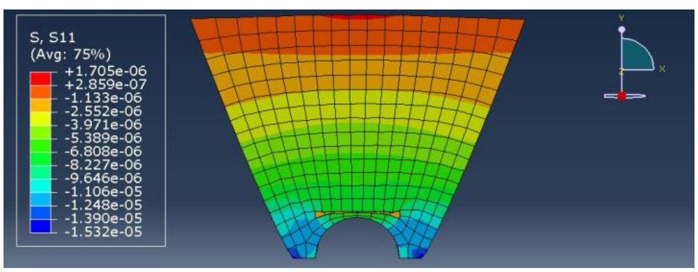

Figure 10: Contours of average LEP for the base conditions.

5.2. Lateral Earth Pressure (LEP) Estimation on the HFCCT for the Study Model with Load Reduction Method Using EPS Geofoam in a Horizontal Formation

Figure 11 presents the relationships of the average LEP on the top of the HFCCT study model with the EPS thickness (in a horizontal formation) and the distance between the bottom of the EPS and the top of the HFCCT. In general, the average LEP on the HFCCT is reduced with the increase in EPS thickness. For the majority of EPS thicknesses, the best results of LEP reduction were achieved with a 1.0 m distance between the bottom of the EPS and the top of the HFCCT. The best result of using this method of LEP reduction is obtained using 2.5 m EPS thickness and 1.0 m distance between the bottom of EPS and the top of the HFCCT, where the average LEP on the HFCCT reduced from 303 kPa to 170.2 kPa (43.828% reduction in the average LEP on the HFCCT) (see Figures 11 and 12).

Using EPS in a horizontal formation leads the interior soil prism within the HFCCT structure width to settle more than the surrounding exterior sides soil prisms due to the EPS deformation (see Figures 13 and 14), the interior soil prism within the HFCCT structure width deform as a reverse arch-shape. The reduced VEP amount on the HFCCT structure is equal to the shear force on the interior soil prism, which will lead the LEP to be reduced as the LEP value mainly depends on γh.

The results of this method of LEP reduction indicate that the increase in distance between the EPS bottom and the top of the HFCCT has a positive effect on the LEP reduction on the HFCCT. Therefore, for this method, the optimum distance is the highest distance between the EPS bottom and the top of the HFCCT.

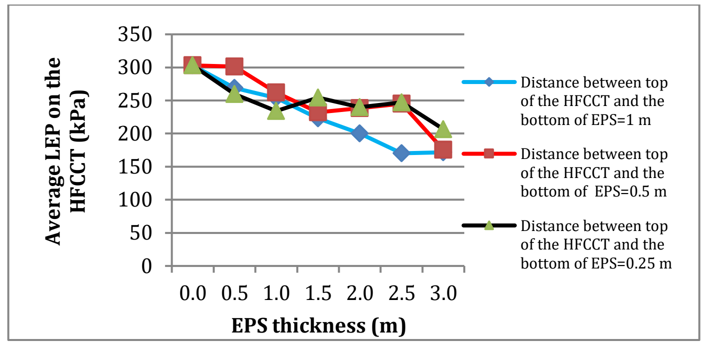

Figure 11: The relationship of the average LEP on top of the HFCCT study model with the EPS thickness (EPS is in a horizontal formation) and the distance between the bottom of the EPS and the top of the HFCCT.

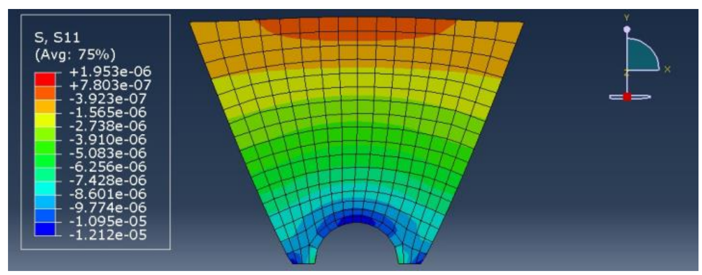

Figure 12: Contours of average lateral earth pressure (LEP) for the best result of using EPS geofoam in a horizontal formation as a method of LEP reduction on the HFCCT.

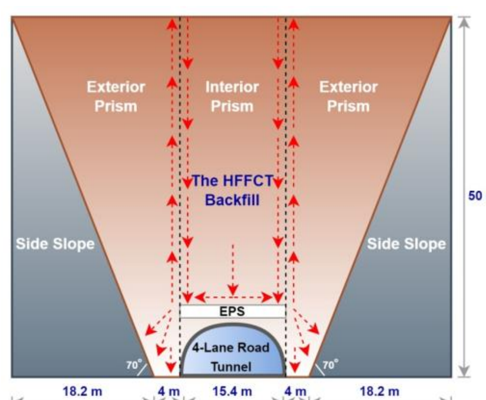

Figure 13: The effect of using EPS geofoam in a horizontal formation on the VEP reduction on the HFCCT study model.

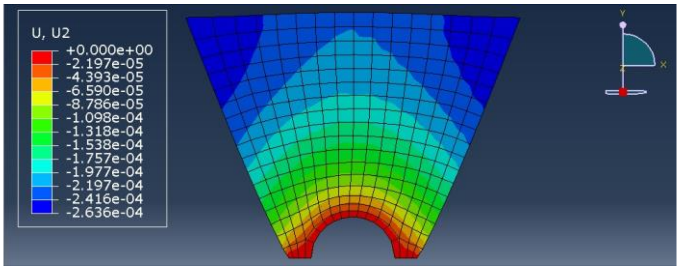

(a)

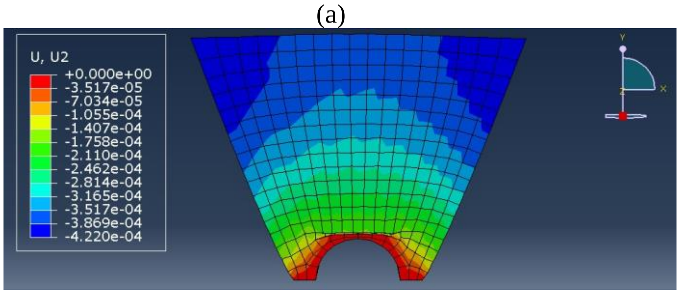

(b)

Figure 14: Contours of: (a) Vertical displacement for the base conditions (no-load reduction method used), (b) Vertical displacement for the best result of using EPS geofoam in a horizontal formation as a method of LEP reduction on the HFCCT.

5.3. Lateral Earth Pressure (LEP) Estimation on the HFCCT for the Study Model with Load Reduction Method Using EPS Geofoam in an Arch Formation

Figure 15 presents the relationships of the average LEP on the top of the HFCCT study model with the EPS thickness (in an arch formation) and the distance between the bottom of the EPS and the top of the HFCCT. In general, the average LEP on the HFCCT is reduced with the increase in EPS thickness. For half of the EPS thicknesses, the best results of LEP reduction were achieved with a 1.0 m distance between the bottom of the EPS and the top of the HFCCT. The best result of using this method of LEP reduction is obtained using 3.0 m EPS thickness and 1.0 m distance between the bottom of EPS and the top of the HFCCT, where the average LEP on the HFCCT reduced from 303 kPa to 160.75 kPa (46.947% reduction in the average LEP on the HFCCT) (see Figures 15 and 16).

Using EPS in an arch formation leads the interior soil prism within the HFCCT structure width to settle more than the surrounding exterior sides soil prisms due to the EPS deformation (see Figures 17 and 18), the interior soil prism within the HFCCT structure width deform as a reverse arch-shape. The reduced VEP amount on the HFCCT structure is equal to the shear force on the interior soil prism, which will lead the LEP to be reduced as the LEP value mainly depends on γh. The idea of using the EPS in an arch formation was to reduce more VEP on the HFCCT by dissipating more VEP to the sides exterior soil prisms and then to the side slopes of the valley through increasing the soil arching effect that forms in the backfill of the HFCCT.

The results of this method indicate that the increase in distance between the EPS bottom and the top of the HFCCT has a positive effect on the LEP reduction on the HFCCT. Therefore, for this method, the optimum distance is the highest distance between the EPS bottom and the top of the HFCCT.

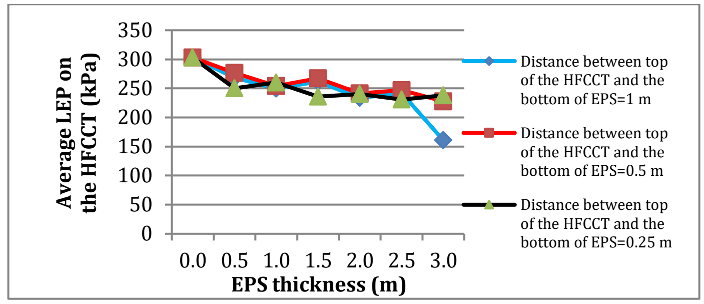

Figure 15: The relationship of the average LEP on top of the HFCCT study model with the EPS thickness (EPS is in an arch formation) and the distance between the bottom of the EPS and the top of the HFCCT.

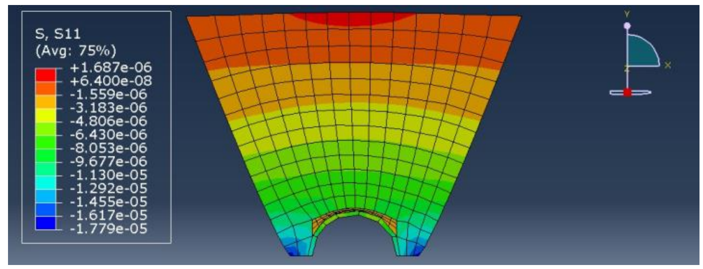

Figure 16: Contours of average lateral earth pressure (LEP) for the best result of using EPS geofoam in an arch formation as a method of LEP reduction on the HFCCT.

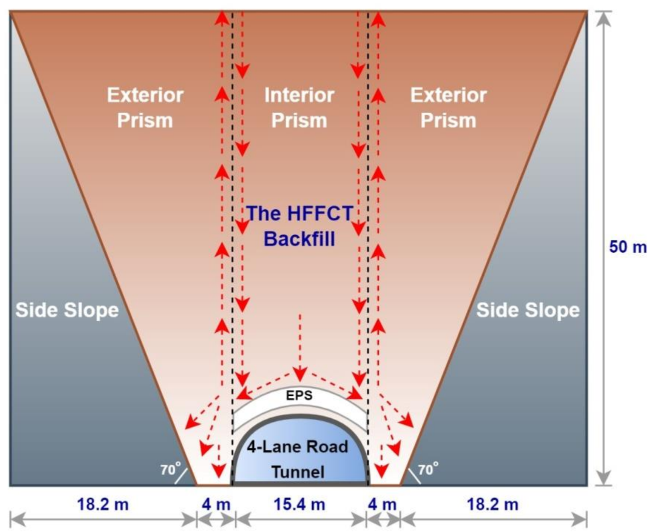

Figure 17: The effect of using EPS geofoam in an arch formation on the VEP reduction on the HFCCT study model.

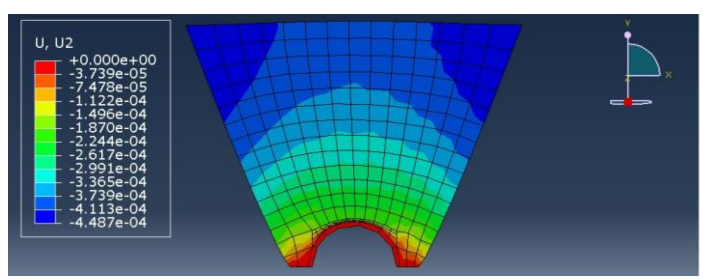

Figure 18: Contours of vertical displacement for the best result of using EPS geofoam in an arch formation as a method of LEP reduction on the HFCCT.

5.4. Lateral Earth Pressure (LEP) Estimation on the HFCCT for the Study Model with Load Reduction Method Using EPS Geofoam in a Combined Horizontal and Arch Formation

Figure 19 presents the relationships of the average LEP on the top of the HFCCT study model with the EPS thickness (in a combined horizontal and arch formation) and the distance between the bottom of the EPS and the top of the HFCCT. In general, the average LEP on the HFCCT is reduced with the increase of EPS thickness until the EPS thickness reaches 2.0 m, where the LEP starts to increase when the EPS thickness increases above 2.0 m. For all of the EPS thicknesses, the best results of LEP reduction were achieved with a 1.0 m distance between the bottom of the EPS and the top of the HFCCT. The best result of using this method of LEP reduction on the HFCCT is obtained using 2.0 m EPS thickness and 1.0 m distance between the bottom of EPS and the top of the HFCCT, where the average LEP on the HFCCT reduced from 303 kPa to 158.6 kPa (47.656% reduction in the average LEP on the HFCCT) (see Figures 19 and 20).

Using EPS in a combined horizontal and arch formation leads the interior soil prism within the HFCCT structure width to settle more than the surrounding exterior sides soil prisms due to the EPS deformation (see Figures 21 and 22), the interior soil prism within the HFCCT structure width deform as a reverse arch-shape. The reduced VEP amount on the HFCCT structure is equal to the shear force on the interior soil prism, which will lead the LEP to be reduced as the LEP value mainly depends on γh. The idea of using the EPS in a combined horizontal and arch formation was to reduce more VEP on the HFCCT by dissipating more VEP to the sides exterior soil prisms and then to the side slopes of the valley through increasing the soil arching effect that forms in the backfill of the HFCCT.

The results of this method indicate that the increase in distance between the EPS bottom and the top of the HFCCT has a positive effect on the LEP reduction on the HFCCT. Therefore, the optimum distance is the highest distance between the EPS bottom and the top of the HFCCT.

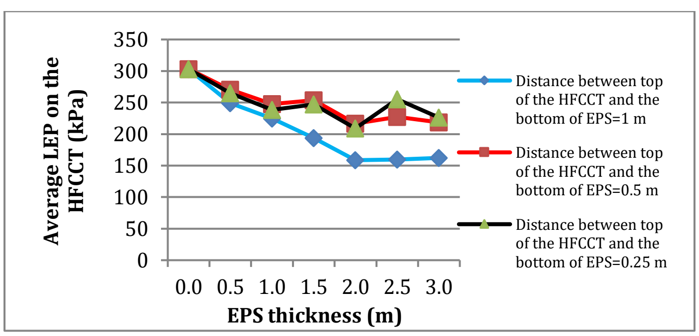

Figure 19: The relationship of the average LEP on top of the HFCCT study model with the EPS thickness (in a combined horizontal and arch formation) and the distance between the bottom of the EPS and the top of the HFCCT.

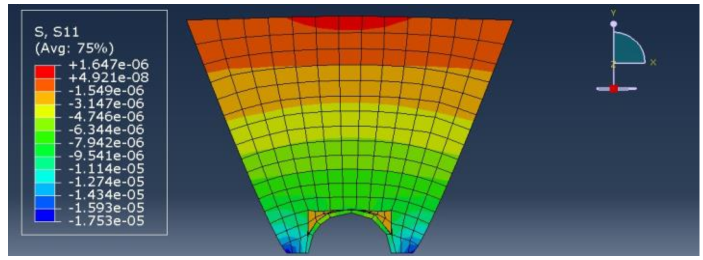

Figure 20: Contours of average lateral earth pressure (LEP) for the best result of using EPS geofoam in a combined horizontal and arch formation as a method of LEP reduction on the HFCCT.

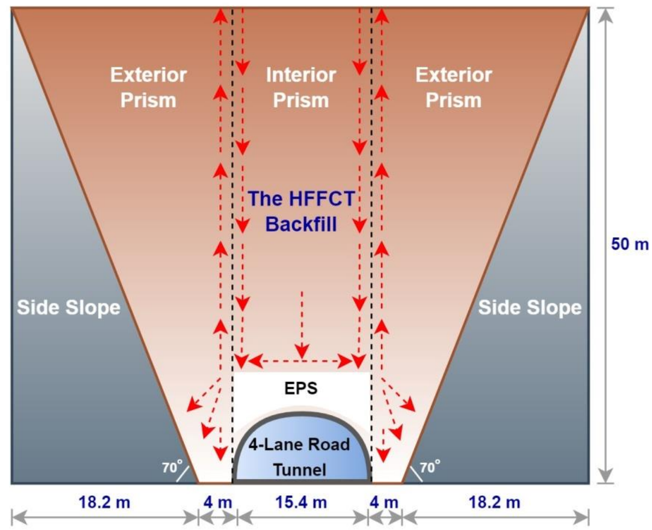

Figure 21: The effect of using EPS geofoam in a combined horizontal and arch formation on the VEP reduction on the HFCCT study model.

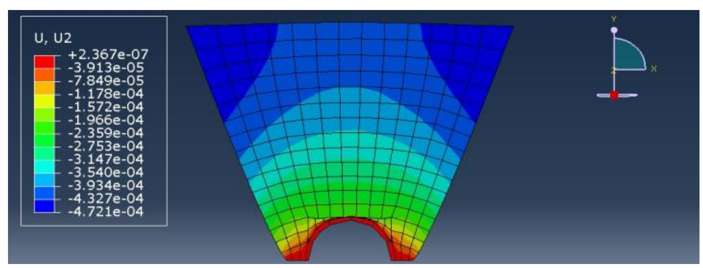

Figure 22: Contours of vertical displacement for the best result of using EPS geofoam in a combined horizontal and arch formation as a method of LEP reduction on the HFCCT.

5.5. Lateral Earth Pressure (LEP) Estimation on the HFCCT for the Study Model with Load Reduction Method Using TDA in a Horizontal Formation

Figure 23 presents the relationships of the average LEP on the top of the HFCCT study model with the TDA thickness (in a horizontal formation) and the distance between the bottom of the TDA and the top of the HFCCT. In general, the average LEP on the HFCCT is reduced with the increase of TDA thickness. For half of the TDA thicknesses, the best results of LEP reduction were achieved with a 0.5 m distance between the bottom of the TDA and the top of the HFCCT. The best result of this method of LEP reduction is obtained using 3.0 m TDA thickness and 0.25 m distance between the bottom of TDA and the top of the

HFCCT, where the average LEP on the HFCCT reduced from 303 kPa to 80.125 kPa (73.556% reduction in the average LEP on the HFCCT) (see Figures 23 and 24).

Using TDA in a horizontal formation leads the interior soil prism within the HFCCT structure width to settle more than the surrounding exterior sides soil prisms due to the TDA deformation (see Figures 25 and 26), the interior soil prism within the HFCCT structure width deforms as a reverse arch-shape. The reduced VEP amount on the HFCCT structure is equal to the shear force on the interior soil prism, which will lead the LEP to be reduced as the LEP value mainly depends on γh.

The results of this method of LEP reduction indicate that the increase in distance between the TDA bottom and the top of the HFCCT has a positive effect on the LEP reduction on the HFCCT. In this method of LEP reduction, the optimum distance between the TDA bottom and the top of the HFCCT can be estimated from the results of using this method, and it is not necessarily the shortest or highest distance between the TDA bottom and the top of the HFCCT.

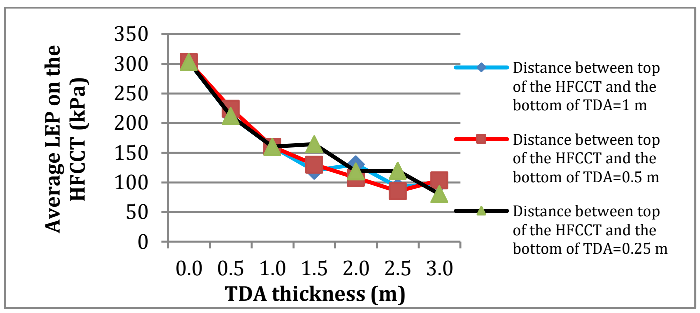

Figure 23: The relationship of the average LEP on top of the HFCCT study model with the TDA thickness (in a horizontal formation) and the distance between the bottom of the TDA and the top of the HFCCT.

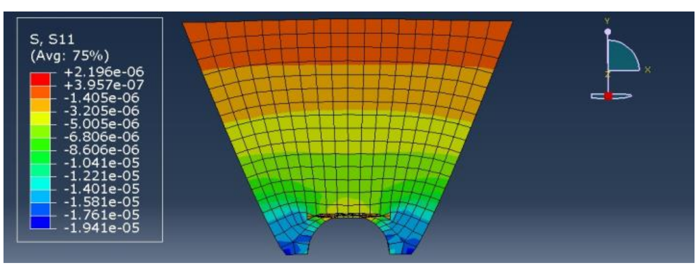

Figure 24: Contours of average lateral earth pressure (LEP) for the best result of using TDA in a horizontal formation as a method of LEP reduction on the HFCCT

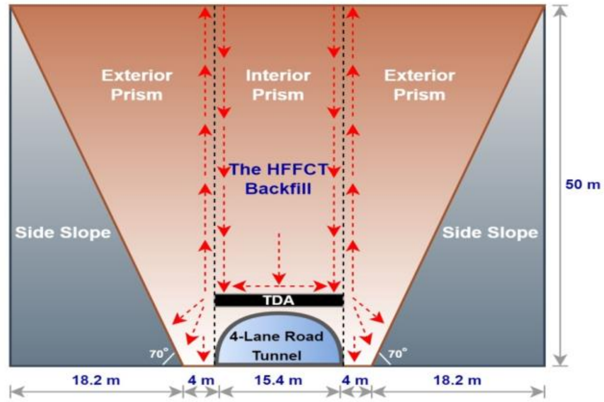

Figure 25: The effect of using TDA in a horizontal formation on the VEP reduction on the HFCCT study model

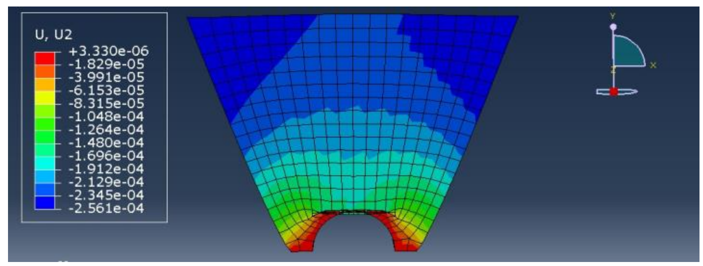

Figure 26: Contours of vertical displacement for the best result of using TDA in a horizontal formation as a method of LEP reduction on the HFCCT.

5.6. Lateral Earth Pressure (LEP) Estimation on the HFCCT for the Study Model with Load Reduction Method Using TDA in an Arch Formation

Figure 27 presents the relationships of the average LEP on the top of the HFCCT study model with the TDA thickness (in an arch formation) and the distance between the bottom of the TDA and the top of the HFCCT. For most of the TDA thicknesses, the best results of LEP reduction were achieved with a 1.0 m distance between the bottom of the TDA and the top of the HFCCT. The best result of using this method of LEP reduction on the HFCCT is obtained using 3.0 m TDA thickness and 1.0 m distance between the bottom of TDA and the top of the HFCCT, where the average LEP on the HFCCT reduced from 303 kPa to 185.325 kPa (38.836% reduction in the average LEP on the HFCCT) (see Figures 27 and 28).

Using TDA in an arch formation leads the interior soil prism within the HFCCT structure width to settle more than the surrounding exterior sides soil prisms due to the TDA deformation (see Figures 29 and 30), the interior soil prism within the HFCCT structure width deforms as a reverse arch-shape. The reduced VEP amount on the HFCCT structure is equal to the shear force on the interior soil prism, which will lead the LEP to be reduced as the LEP value mainly depends on γh. The idea of using the TDA in an arch formation was to reduce more VEP on the HFCCT by dissipating more VEP to the sides exterior soil prisms and then to the side slopes of the valley through increasing the soil arching effect that forms in the backfill of the HFCCT.

The results of this method indicate that the increase in distance between the TDA bottom and the top of the HFCCT has a positive effect on the LEP reduction on the HFCCT. Therefore, the optimum distance is the highest distance between the TDA bottom and the top of the HFCCT.

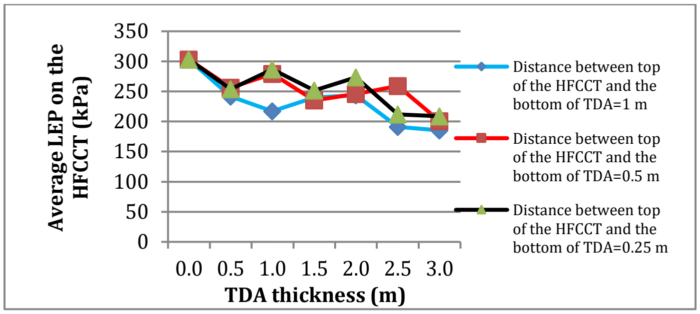

Figure 27: The relationship of the average LEP on top of the HFCCT study model with the TDA thickness (in an arch formation) and the distance between the bottom of the TDA and the top of the HFCCT.

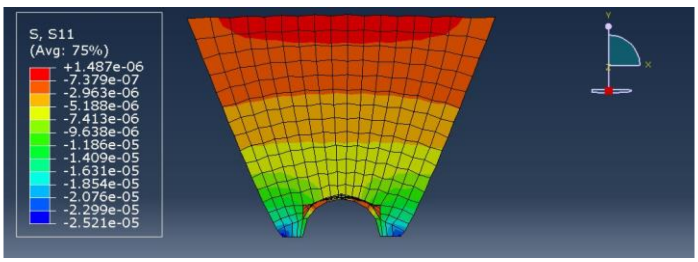

Figure 28: Contours of average lateral earth pressure (LEP) for the best result of using TDA in an arch formation as a method of LEP reduction on the HFCCT.

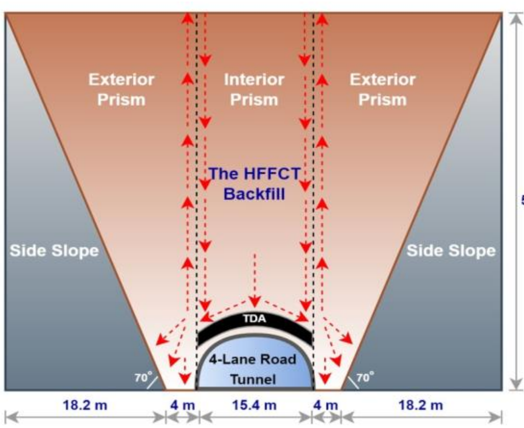

Figure 29: The effect of using TDA in an arch formation on the VEP reduction on the HFCCT study model.

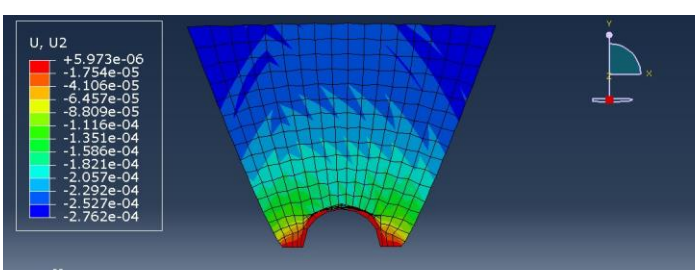

Figure 30: Contours of vertical displacement for the best result of using TDA in an arch formation as a method of LEP reduction on the HFCCT

5.7 Lateral Earth Pressure (LEP) Estimation on the HFCCT for the Study Model with Load Reduction Method Using TDA in a Combined Horizontal and Arch Formation

Figure 31 presents the relationships of the average LEP on the top of the HFCCT study model with the TDA thickness (in a combined horizontal and arch formation) and the distance between the bottom of the TDA and the top of the HFCCT. For most of the TDA thicknesses, the best results of LEP reduction were achieved with a 1.0 m distance between the bottom of the TDA and the top of the HFCCT. The best result of using this method of LEP reduction on the HFCCT is obtained using 3.0 m TDA thickness and 0.5 m distance between the bottom of TDA and the top of the HFCCT, where the average LEP on the HFCCT reduced from 303 kPa to 95.2 kPa (68.58% reduction in the average LEP on the HFCCT) (see Figures 31and 32).

Using TDA in a combined horizontal and arch formation leads the interior soil prism within the HFCCT structure width to settle more than the surrounding exterior sides soil prisms due to the TDA deformation (see Figures 33 and 34), the interior soil prism within the HFCCT structure width deform as a reverse arch-shape. The reduced VEP amount on the HFCCT structure is equal to the shear force on the interior soil prism, which will lead the LEP to be reduced as the LEP value mainly depends on γh. The idea of using the TDA in a combined horizontal and arch formation was to reduce more VEP on the HFCCT by dissipating more VEP to the sides exterior soil prisms and then to the side slopes of the valley through increasing the soil arching effect that forms in the backfill of the HFCCT.

The results of this method indicate that the optimum distance between the TDA bottom and the top of the HFCCT has a positive effect on the LEP reduction on the HFCCT. In this method of LEP reduction, the optimum distance between the TDA bottom and the top of the HFCCT can be estimated from the results of using this method, and it is not necessarily the shortest or highest distance between the TDA bottom and the top of the HFCCT.

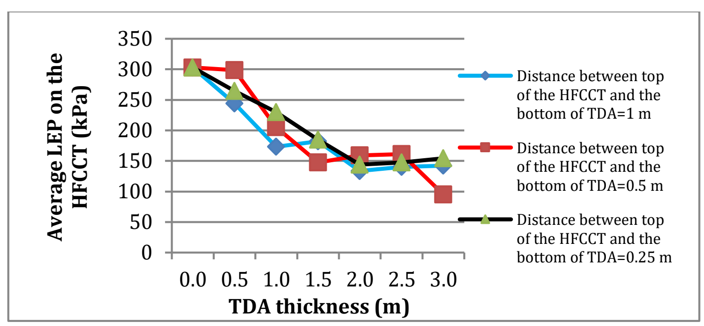

Figure 31: The relationship of the average LEP on top of the HFCCT study model with the TDA thickness (in a combined horizontal and arch formation) and the distance between the bottom of the TDA and the top of the HFCCT

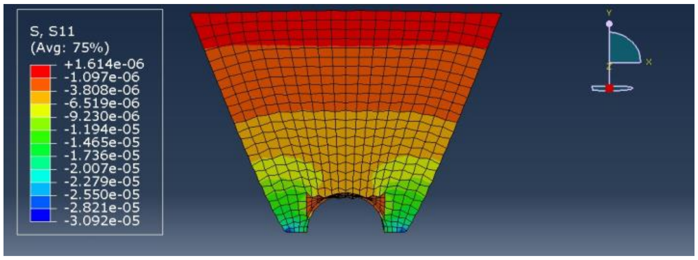

Figure 32: Contours of average lateral earth pressure (LEP) for the best result of using TDA in a combined horizontal and arch formation as a method of LEP reduction on the HFCCT.

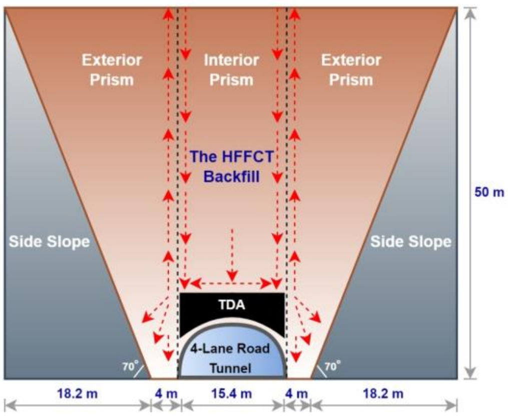

Figure 33: The effect of using TDA in a combined horizontal and arch formation on the VEP reduction on the HFCCT study model.

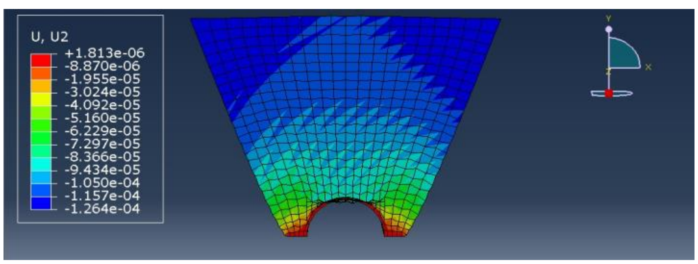

Figure 34: Contours of vertical displacement for the best result of using TDA in a combined horizontal and arch formation as a method of LEP reduction on the HFCCT.

6. Analytical Estimation of Lateral Earth Pressure (LEP)

According to previous studies for vertical earth pressure (VEP), lateral earth pressure (LEP) can be derived based on the analytical solution for LEP (Rankine equation for active lateral earth pressure) [41]. To consider all the significant and influential factors of LEP distribution that are applicable to an HFCCT, and simplify the use of the analytical equations, the modified LEP coefficient, $\lambda_{modified}$ is introduced. Then the LEP, σ, and the modified LEP coefficient, $\lambda_{modified}$ will be expressed as Equations (3) and (4) [42].

$$\sigma = \lambda_{modified}\, \gamma h \qquad (3)$$

$$\lambda_{modified} = f(S, D, M, \theta, B, \lambda) \qquad (4)$$

Where:

B: the width of the valley floor.
D: the width of CCT.
h: the height of backfill above the CCT (m).
M: the effect of the mechanical properties of the backfill materials.
S: the effect of the cross-sectional shape of the CCT.
γ: unit weight of backfill soil (kN/m^3).
λ: the LEP on side of CCT in specification (Rankine coefficient of active earth pressure),

$$\lambda = \tan^2 (45 - \tfrac{\varphi}{2})$$

φ = friction angle of backfill soil (°).

For the estimation of lateral earth pressure (LEP) on the HFCCT for the base condition of the study model (No load reduction method is used), the Rankine modified equation was used. Where through an analytical model of LEP and a numerical analysis the LEP coefficient, λ, is related to k_0, the cross-sectional shape of the CCT; k_1, properties of the backfill; k_2, the width of the CCT; and k_3, the coupled effect of the slope angle, θ, and the valley width to the width of the CCT ratio (the B/D ratio). The LEP coefficient of CCT with rectangular cross-section is greater than the LEP coefficient of CCT with arch cross-section, and the greater LEP acts on the CCT with the greater the elasticity modulus, and if the height of backfill above the CCT to the width of the CCT ratio (h/D ratio) is less than 2.2, the LEP coefficient will be greater for a decrease in D, and the LEP coefficient will reduce with a decrease in D if the h/D ratio is higher than 2.2. The coupled effects of slope angle, θ, and the valley width to the width of the CCT ratio (the B/D ratio) are highly correlated with the induced equivalent LEP. Each of the influential factors can be obtained by regression and a modified LEP coefficient, $\lambda_{modified}$ can be proposed by combining all these influential factors. Therefore, the modified coefficient for LEP, $\lambda_{modified}$ on the sides of an HFCCT should be calculated using Equation (5).

$$\lambda_{modified} = k_0 \,.\, k_1 \,.\, k_2 \,.\, k_3 \,.\, \lambda \qquad (5)$$

k_0, k_1, k_2 and k_3 coefficients are calculated using the following equations:

$$k_0 = (-\,0.0115D + 1.4187)\left(\frac{h}{D}\right)^{(-0.0113D-0.0482)} \qquad (6)$$

Where k_0 = 1.0 when the cross-section of the CCT is an arch and k_0 is calculated by Equation (7) when the cross-section is a rectangle.

$$k_1 = k_{1E}\, k_{1C}\, k_{1F} \qquad (7)$$

Where:

$$k_{1E} = [(0.0011\ D + 0.0029)\ \ln(E) - (0.0009\ D + 0.004)]\,\frac{h}{D} + (1.1326 - 0.0229D)\ E^{(0.0102D-0.0338)} \qquad (8)$$

Four different backfill cohesion values were examined: c = 31.11 kPa, 40 kPa, 50 kPa, and 60 kPa. k_{1C} is the coefficient for modifying the cohesion of the backfill effect; the equivalent LEP coefficients are listed in Table 9, showing that the variation in values is limited for the different cohesion values. The results indicate that k_{1C} is independent of cohesion. Therefore, for any HFCCT, k_{1C} = 1.0 regardless of the backfill cohesion, which means that the effect of cohesion on LEP can be neglected or ignored for HFCCTs.

Table 9: Equivalent lateral earth pressure coefficients for different backfill cohesion (c) values [42].

Height of Backfill, (m)	c = 31.11 kPa	c = 40 kPa	c = 50 kPa	c = 60 kPa
5	0.26	0.27	0.27	0.27
10	0.31	0.30	0.29	0.29
15	0.34	0.33	0.32	0.32
20	0.35	0.34	0.34	0.33
25	0.35	0.35	0.35	0.34
30	0.36	0.35	0.35	0.35
35	0.36	0.36	0.35	0.35
40	0.36	0.36	0.36	0.35
45	0.36	0.36	0.36	0.35
50	0.35	0.35	0.35	0.35

$$k_{1F} = \begin{cases} 1 & \frac{h}{D} \leq 0.75 \\ 0.92 & \frac{h}{D} > 0.75 \end{cases} \quad (9)$$

$$k_2 = \begin{cases} 0.872\left(\frac{h}{D}\right)^{0.178} & \frac{h}{D} \leq 2.2 \\ -0.0138\frac{h}{D} + 1.0318 & \frac{h}{D} > 2.2 \end{cases} \quad (10)$$

$$k_3 = \{[(0.02D - 0.1195) \ln (\tan \Theta) + (0.2841 - 0.0019D)]\frac{B}{D} + [(0.016D + 0.39) - (0.4709 - 0.0097D) \ln (\tan \Theta)]\} \left(\frac{h}{D}\right)^{-q} \quad (11)$$

Where:

$$q = [(0.0078D - 0.0901) \ln (\tan \Theta) + (0.0037D - 0.016)]\frac{B}{D} + [(0.1537 - 0.0096D) \ln (\tan \Theta) + (0.2253 - 0.0082D)] \quad (12)$$

calculation of the lateral earth pressure (LEP) on the HFCCT for the base condition of the study model is done as in the following:

$k_0 = 1.0$ because the cross-section of the CCT of the study model is an arch.

$k_{1E} = [(0.0011 * 15.4 + 0.0029) \ln (11.25) – (0.0009 * 15.4 + 0.004)]\frac{42.3}{15.4} + (1.1326 - 0.0229 * 15.4)\ 11.25^{(0.0102*15.4-0.0338)} = 0.04802 – 0.04905 + 1.05110 = 1.05$

$k_{1C} = 1.0$

$\frac{h}{D} = \frac{42.3}{15.4} = 2.746 > 0.75 \quad \therefore k_{1F} = 0.92$

$k_1 = 1.05 * 1.0 * 0.92 = 0.966$

$\frac{h}{D} = \frac{42.3}{15.4} = 2.746 > 2.2 \quad \therefore k_2 = -0.0138\frac{42.3}{15.4} + 1.0318 = 0.993$

$q = \{[(0.0078 * 15.4 - 0.0901) \ln (\tan 70) + (0.0037 * 15.4 - 0.016)]\frac{23.4}{15.4} + [(0.1537 - 0.0096 * 15.4) \ln (\tan 70) + (0.2253 - 0.0082 * 15.4)]\} = (0.03034 + 0.0409) * 1.5194 + (0.005922 + 0.09902) = 0.2131$

$k_3 = \{[(0.02 * 15.4 - 0.1195) \ln (\tan 70) + (0.2841 - 0.0019 * 15.4)]\frac{23.4}{15.4} + [(0.016 * 15.4 + 0.39) – (0.4709 - 0.0097 * 15.4) \ln (\tan 70)]\} \left(\frac{42.3}{15.4}\right)^{-0.2131} = [(0.1905 + 0.2548) * 1.5194 + (0.6364 – 0.3249)] * 0.8062 = 0.7965$

$\lambda = \tan^2 (45 - \frac{36}{2}) = 0.2596$

$\lambda_{modified} = 1.0 * 0.966 * 0.993 * 0.7965 * 0.2596 = 0.1983$

$\sigma = 0.1983 * 18.7 * 42.3 = 156.85$ kPa

7. Model Verification

The calculated and estimated LEP values on the HFCCT study model with the base conditions showed that the calculated value using the Rankine modified equation is 23.61% lower than the calculated value using the Rankine equation for active lateral earth pressure, which is a high percentage of difference. The estimated value using Abaqus CAE 2019 is 47.56% higher than the calculated value using the Rankine equation for active lateral earth pressure, which is also a high percentage of difference (see Table 10).

Rankine modified equation is a modification of the Rankine equation for active lateral earth pressure ($\sigma = \lambda\ \gamma h$) using the ANSYS finite element code to investigate the influences of each of the factors; S, D, M, θ, and B which were mentioned previously through four proposed corresponding coefficients, k_0, k_1, k_2 and k_3. For the HFCCT study model with the base conditions, by adding the effect of S, D, M, θ, and B to the Rankine equation for active lateral earth pressure through Rankine modified equation, the LEP on the HFCCT reduced from 205.34 kPa to 156.85 kPa. On the other hand, the estimated LEP value using Abaqus CAE 2019 is higher than the calculated value of the LEP using the Rankine equation for active lateral earth pressure, and the difference between the two values of the LEP is 47.56% (see Table 10).

Table 10: The calculation and estimation of lateral earth pressure (LEP) on the HFCCT for the base conditions of the study model (No load reduction method is used) using analytical and numerical methods.

Method of LEP calculation	LEP (kPa)	The percentage of the difference with Rankine active lateral earth pressure (%)
Rankine equation for active lateral earth pressure ($\sigma = \lambda\ \gamma h$)	205.34	-
Rankine modified equation ($\sigma = \lambda_{modified}\ \gamma h$)	156.85	-23.61
Complete Abaqus Environment 2019 Software (Abaqus CAE 2019)	303	+47.56

Conclusion

This study used Abaqus CAE 2019 software, which is based on the finite element method, to investigate the effect of using EPS geofoam and TDA in different forms on the LEP reduction on the HFCCT due to the relative vertical displacements of the HFCCT backfill soil prisms and soil arching. Several influential factors, including the formation of the EPS and the TDA, the thickness of the EPS and TDA, and the distance between the top of the HFCCT and the bottom of the EPS and the TDA were studied. Also, a comparison is made between the calculated and estimated LEP values on the HFCCT study model with the base conditions using the Rankine equation for active lateral earth pressure, Rankine modified equation, and Abaqus CAE 2019 software. Therefore, several conclusions can be drawn from this study:

1. Concerning LEP reduction on the HFCCT, the presence of EPS and TDA in different formations on top of an HFCCT can transfer the load from the top to the sides of the HFCCT and then to the sides slopes, thereby reducing the VEP on the HFCCT due to soil arching and the relative vertical displacements of the HFCCT backfill soil prisms, which will lead the LEP to be reduced as the LEP value mainly depends on γh.

2. The best result of EPS presence on the top of an HFCCT is achieved using the EPS geofoam in a combined horizontal and arch formation as a method of LEP reduction on the HFCCT. This result is achieved by using 2.0 m EPS thickness and 1.0 m distance between the top of the HFCCT and the bottom of EPS, where the average LEP on the HFCCT reduced from 303 kPa to 158.6 kPa (47.656% reduction in the average LEP on the HFCCT).

3. The best result of TDA presence on the top of an HFCCT is achieved using the TDA in a horizontal formation as a method of LEP reduction on the HFCCT. This result is achieved by using 3.0 m TDA thickness and 0.25 m distance between the top of the HFCCT and the bottom of TDA, where the average LEP on the HFCCT reduced from 303 kPa to 80.125 kPa (73.556% reduction in the average LEP on the HFCCT).

4. Reducing the LEP on the HFCCT will lead the internal forces of the HFCCT lining structure to decrease. Then, the required design thickness of the HFCCT lining structure can be minimized and improve the safety of the HFCCT when it is subjected to high LEP.

5. The presence of the TDA material as a compressible material on the top of the HFCCT for load reduction purposes can help clean the environment by using large amounts of the scrap vehicles' tires in the form of TDA material.

This research has revealed the following opportunities for future work:

1. Using EPS geofoam in different forms with the presence of concrete canvas above the EPS geofoam on top of the HFCCTs as methods of load reduction on HFCCTs.
2. Using TDA in different forms with the presence of concrete canvas above the TDA on top of the HFCCTs as methods of load reduction on HFCCTs.

Conflict of interests

Conflict of interests

There is no conflict of interest.

Author Contribution

As a Ph.D. student, Shamil Arkawazi contributed most of the works including writing of the manuscript, and Dr. Mohammad Hajiazizi as a supervisor of the Ph.D. student Shamil Arkawazi reviewed the manuscript and contributed to the content and discussion. All authors have read and agreed to the published version of the manuscript.

Funding Information

The authors received no direct or un-direct funding for this research.

References

1. M. A and A. AO, *The theory of loads on pipes in ditches and tests of cement and clay drain tile and sewer pipe*. 1913.
2. M. G. Marston, "The Theory of External Loads on Closed Conduits in the Light of the Latest Experiments," *Highw. Res. Board Proceeding*, vol. 9, pp. 138–170, 1930, [Online]. Available: https://trid.trb.org/view/103945.
3. M. G. Spangler, "A PRACTICAL APPLICATION OF THE IMPERFECT DITCH METHOD OF CONSTRUCTION," *Washington, DC Highw. Res. Board.*, vol. 37 of Proc, no. 37th Annual Meeting of the Highway Research Board, pp. 271–277, 1958.
4. R. K. Taylor, "Induced-Trench Method of Culvert Installation.," *Highw Res. Rec.*, no. 443, pp. 15–31, 1973.
5. J. A. Sladen and J. M. Oswell, "The induced trench method - a critical review and case history," *Can. Geotech. J.*, vol. 25, no. 3, pp. 541–549, 1988, doi: 10.1139/t88-059.
6. J. Vaslestad, T. H. Johansen, and W. Holm, "Load reduction on rigid culverts beneath high fills: long-term behavior," *Transp. Res. Rec.*, no. 1415, pp. 58–68, 1993.
7. A. Q. Gu, T. T. Guo, and X. P. Wang., "Experimental study on reducing load measurement using EPS of culvert under high-stacked soil," *Chinese J. Geotech. Eng.*, vol. 27, no. 5, p. 2005, 2005.
8. R. P. McAffee and A. J. Valsangkar, "Field performance, centrifuge testing, and numerical modelling of an induced trench installation," *Can. Geotech. J.*, vol. 45, no. 1, pp. 85–101, 2008, doi: 10.1139/T07-086.
9. B. L. McGuigan and A. J. Valsangkar, "Centrifuge testing and numerical analysis of box culverts installed in induced trenches," *Can. Geotech. J.*, vol. 47, no. 2, pp. 147–163, 2010, doi: 10.1139/T09-085.
10. S. Li, I. H. Ho, L. Ma, Y. Yao, and C. Wang, "Load reduction on high-filled cut-and-cover tunnel using discrete element method," *Comput. Geotech.*, vol. 114, no. March, 2019, doi: 10.1016/j.compgeo.2019.103149.
11. J. Kang, F. Parker, and C. H. Yoo, "Soil-Structure Interaction and Imperfect Trench Installations for Deeply Buried Concrete Pipes," *J. Geotech. Geoenvironmental Eng.*, vol. 133, no. 3, pp. 277–285, 2007, doi: 10.1061/(asce)1090-0241(2007)133:3(277).
12. S. Li, G. Han, I.-H. Ho, L. Ma, Q. Wang, and B. Yu, "Coupled Effect of Cross-Sectional Shape and Load Reduction on High-Filled Cut-and-Cover Tunnels Considering Soil–Structure Interaction," *Int. J. Geomech.*, vol. 20, no. 7, p. 04020082, 2020, doi: 10.1061/(asce)gm.1943-5622.0001696.
13. S. Li, Y. Yao, I.-H. Ho, L. Ma, Q. Wang, and C. Wang, "Coupled Effect of Expanded Polystyrene and Geogrid on Load Reduction for High-Filled Cut-and-Cover Tunnels Using the Discrete-Element Method," *Int. J. Geomech.*, vol. 20, no. 6, p. 04020052, 2020, doi: 10.1061/(asce)gm.1943-5622.0001683.

14. L. M. Rodríguez, M. Arroyo, and M. M. Cano, “Use of tire derived aggregate in tunnel cut-and-cover,” *Can. Geotech. J.*, vol. 55, pp. 1–32, 2018, doi: https://doi.org/10.1139/cgj-2017-0446.

15. S. A. F. Arkawazi and M. Hajiazizi, “Coupled effect of tire-derived aggregate and geogrid on lateral earth pressure on high-filled cut-and-cover tunnels,” vol. 1, pp. 73–87, 2023, doi: 10.22059/IJMGE.2022.346697.594987.

16. B. Zhuo, F. Wang, Y. Fang, Y. Chen, and G. Ning, “Analysis of Cracking Development and Mechanical Characteristics of High-Filled Cut-and-Cover Tunnel,” *KSCE J. Civ. Eng.*, vol. 24, no. 8, pp. 2519–2532, 2020, doi: 10.1007/s12205-020-0247-3.

17. W. S. Jutkofsky, J. T. Sung, and D. Negussey, “Stabilization of Embankment Slope with Geofoam,” *Transp. Res. Rec.*, no. 00, pp. 94–102, 2000.

18. C. B. Farnsworth *et al.*, “Rapid Construction and Settlement Behavior of Embankment Systems on Soft Foundation Soils,” *J. Geotech. GEOENVIRONMENTAL Eng.*, no. March, pp. 289–301, 2008, doi: 10.1061/_ASCE_1090-0241_2008_134:3_289.

19. J. S. Horvath, “The Compressible Inclusion Function of EPS Geofoam,” *Geotext. Geomembranes*, vol. 15, no. 1997, pp. 77–120, 1998.

20. J. S. Horvath, “Geofoam Compressible Inclusions: The New Frontier In Earth Retaining Structures,” *ASCE*, 2004.

21. R. J. Bathurst, S. Zarnani, and A. Gaskin, “Shaking table testing of geofoam seismic buffers,” *Soil Dyn. Earthq. Eng.*, vol. 27, pp. 324–332, 2007, doi: 10.1016/j.soildyn.2006.08.003.

22. S. Zarnani and R. J. Bathurst, “Experimental investigation of EPS geofoam seismic buffers using shaking table tests,” *Geosynth. Int.*, no. 3, 2007, doi: 10.1680/gein.2007.14.3.165.

23. S. Zarnani and R. J. Bathurst, “Numerical modeling of EPS seismic buffer shaking table tests,” *Geotext. Geomembranes*, vol. 26, pp. 371–383, 2008, doi: 10.1016/j.geotexmem.2008.02.004.

24. K. Hatami and A. F. Witthoeft, “A numerical study on the use of geofoam to increase the external stability of reinforced soil walls,” *Geosynth. Int.*, vol. 15, no. 6, pp. 452–470, 2008, doi: 10.1680/gein.2008.15.6.452.

25. A. Ossa and M. P. Romo, “Geotextiles and Geomembranes Dynamic characterization of EPS geofoam,” *Geotext. Geomembranes*, vol. 29, no. 1, pp. 40–50, 2011, doi: 10.1016/j.geotexmem.2010.06.007.

26. M. Dugkov, “Materials Research on EPS20 and EPS15 Under Representative Conditions in Pavement Structures,” *Geotext. Geomembranes*, vol. 15, no. 1997, pp. 147–181, 1998.

27. M. Dugkov and A. Scarpas, “Three-Dimensional Finite Element Analysis of Flexible Pavements with an (Open Joint in the) EPS Sub-Base,” *Geotext. Geomembranes*, vol. 15, no. 1997, pp. 29–38, 1998.

28. T. D. Stark, D. Arellano, and J. S. Horvath, “Geofoam Applications in the Design and Construction of Highway Embankments Prepared for : Submitted by : Urbana , Illinois,” 2004.

29. X. Huang and D. Negussey, “EPS Geofoam Design Parameters for Pavement Structures,” *Geo-Frontiers 2011 © ASCE 2011*, pp. 4544–4554, 2011.

30. H. Gao, J. Liu, and H. Liu, “Geotechnical properties of EPS composite soil,” *Int. J. Geotech. Eng.*, vol. 6362, no. December, 2011, doi: 10.3328/IJGE.2011.05.01.69-77.

31. H. Gao, G. Chen, and Z. Wang, “The Mechanical Behaviors of the Embankment Filled with EPS Composite Soil,” *Adv. Mater. Res.*, vol. 373, pp. 2813–2818, 2012, doi: 10.4028/www.scientific.net/AMR.368-373.2813.

32. B. S. Chun, H.-S. Lim, Myung Sagong, and K. Kim, “Development of a hyperbolic constitutive model for expanded polystyrene (EPS) geofoam under triaxial compression tests,” *Geotext. Geomembranes*, vol. 22, pp. 223–237, 2004, doi: 10.1016/j.geotexmem.2004.03.005.

33. H. Hazarika, “Stress – strain modeling of EPS geofoam for large-strain applications,” *Geotext. Geomembranes*, vol. 24, pp. 79–90, 2006, doi: 10.1016/j.geotexmem.2005.11.003.

34. H. Wong and C. J. Leo, “A simple elastoplastic hardening constitutive model for EPS geofoam,” *Geotext. Geomembranes*, vol. 24, pp. 299–310, 2006, doi: 10.1016/j.geotexmem.2006.03.007.

35. C. J. Leo, M. Kumruzzaman, H. Wong, and J. H. Yin, “Behavior of EPS geofoam in true triaxial compression tests,” *Geotext. Geomembranes*, vol. 26, pp. 175–180, 2008, doi: 10.1016/j.geotexmem.2007.10.005.

36. A. Ossa and M. P. Romo, “Micro- and macro-mechanical study of compressive behavior of expanded polystyrene geofoam,” *Geosynth. Int.*, no. 5, 2009, doi: 10.1680/gein.2009.16.5.327.

37. A. H. Padade and J. N. Mandal, “Behavior of expanded polystyrene (EPS) geofoam under triaxial loading conditions,” *Electron. J. Geotech. Eng.*, vol. 17 S, pp. 2542–2553, 2012.

38. Geosyntec Consultants, “Guidance Manual for Engineering Uses of Scrap Tires,” 2008.

39. D. Cheng, “Usage Guide-Tire-Derived Aggregate (TDA),” California State, 2016.

40. F. H. Kulhawy and P. W. Mayne, “Manual on Estimating Soil Properties for Foundation Design,” 1990.

41. S. Li, L. Ma, I. H. Ho, Q. Wang, B. Yu, and P. Zhou, “Modification of Vertical Earth Pressure Formulas for High Fill Cut-and-Cover Tunnels Using Experimental and Numerical Methods,” *Math. Probl. Eng.*, vol. 2019, 2019, doi: 10.1155/2019/8257157.

42. L. Ma, S. Li, I. H. Ho, Q. Wang, and B. Yu, “Method to Estimate Lateral Earth Pressure on High-Filled Cut-and-Cover Tunnels,” *KSCE J. Civ. Eng.*, vol. 24, no. 3, pp. 975–987, 2020, doi: 10.1007/s12205-020-1060-8.